

Tunable third-harmonic generation from polaritons in the ultrastrong coupling regime

Fábio Barachati,^{1,*} Janos Simon,² Yulia A. Getmanenko,²
Stephen Barlow,² Seth R. Marder,² and Stéphane Kéna-Cohen^{1,†}

¹*Department of Engineering Physics, École Polytechnique de Montréal, Montréal H3C 3A7, QC, Canada*

²*School of Chemistry and Biochemistry and Center for Organic Photonics and Electronics, Georgia Institute of Technology, Atlanta, GA 30332-0400, USA*

(Dated: March 2, 2022)

Strong inter-particle interactions between polaritons have traditionally stemmed from their exciton component. In this work, we impart a strong photonic nonlinearity to a polaritonic mode by embedding a nonlinear polymethine dye within a high-Q all-metal microcavity. We demonstrate nonlinear microcavities operating in the ultrastrong coupling regime with a normalized coupling ratio of 62%, the highest reported to date. When pumping the lower polariton branch, we observe tunable third-harmonic generation spanning the entire visible spectrum, with internal conversion enhancements more than three orders of magnitude larger than in bare films. Transfer matrix calculations indicate that the observed enhancements are consistent with the enhanced pump electric field.

Keywords: Third-harmonic generation, ultrastrong coupling, exciton-polaritons, microcavities, organic semiconductors, cavity QED.

I. INTRODUCTION

Semiconductor microcavities are natural platforms for the study of light-matter interaction due to their ability to confine cavity photons and semiconductor excitons to the same region of space.¹ If their interaction is strong enough, hybrid light-matter states are formed, called upper (UP) and lower (LP) polaritons.^{2,3} They are separated in energy by the vacuum Rabi splitting (Ω_R), which is related to the coupling strength. Much of the interest in the strong light-matter coupling regime stems from the broad range of nonlinear phenomena that can be observed using polaritons, such as parametric scattering, amplification, bistability, soliton formation and superfluidity.^{1,4,5} Most of these phenomena have, however, been restricted to inorganic microcavities at low-temperatures. There, the intrinsic nonlinearity responsible for pairwise scattering, similar to an optical $\chi^{(3)}$, is strong due to the delocalized nature of Wannier-Mott excitons. The large binding energy of organic Frenkel excitons can in principle allow for such phenomena to be observed at room-temperature, but the exciton-exciton nonlinearities inherent to Frenkel excitons tend to be much weaker than in inorganics. To date, only a handful of nonlinear processes have been observed using organic polaritons,^{6–10} including room-temperature superfluidity.¹¹

In the limit where the exciton-photon coupling is increased to a significant fraction of the uncoupled exciton energy ($\Omega_R \sim E_{EX}$), the system enters the so-called ultrastrong coupling regime (USC). In this regime, the presence of non-negligible antiresonant light-matter coupling terms leads to modifications of both excited and ground state properties, a subject which is currently under intense investigation.^{12–14} Demonstrations of USC in organic microcavities^{15–17} have triggered many interesting studies about its effects on observable material

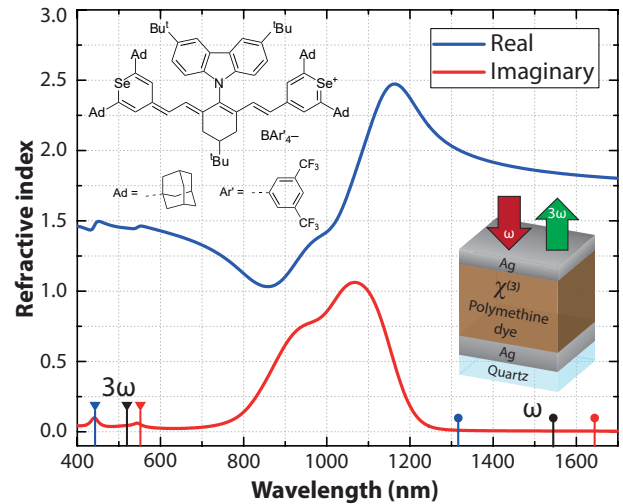


Figure 1. Real (blue) and imaginary (red) refractive index of neat polymethine. The imaginary part has a peak value of 1.06 at 1067 nm. Round (triangular) markers indicate the pump (THG) wavelengths where power dependence measurements were performed. The inset shows (top) the chemical structure of the polymethine dye and counterion and (bottom) a schematic of the microcavity structure.

properties,^{18–20} with many open questions remaining.

In this paper, we demonstrate organic microcavities operating in the USC regime with a Rabi splitting corresponding to a record 62% of the uncoupled exciton energy. The microcavities are composed of a film of a bis(selenopyrylium)-terminated heptamethine dye (see Fig. 1). Dyes of this type exhibit extremely large magnitudes of the molecular third-order polarizability in solution.²¹ The dye used in this study is one of many developed in which bulky substituents on both the chalcogenopyrylium end groups and on the polymethine chain, along with a large counterion, are used to disrupt

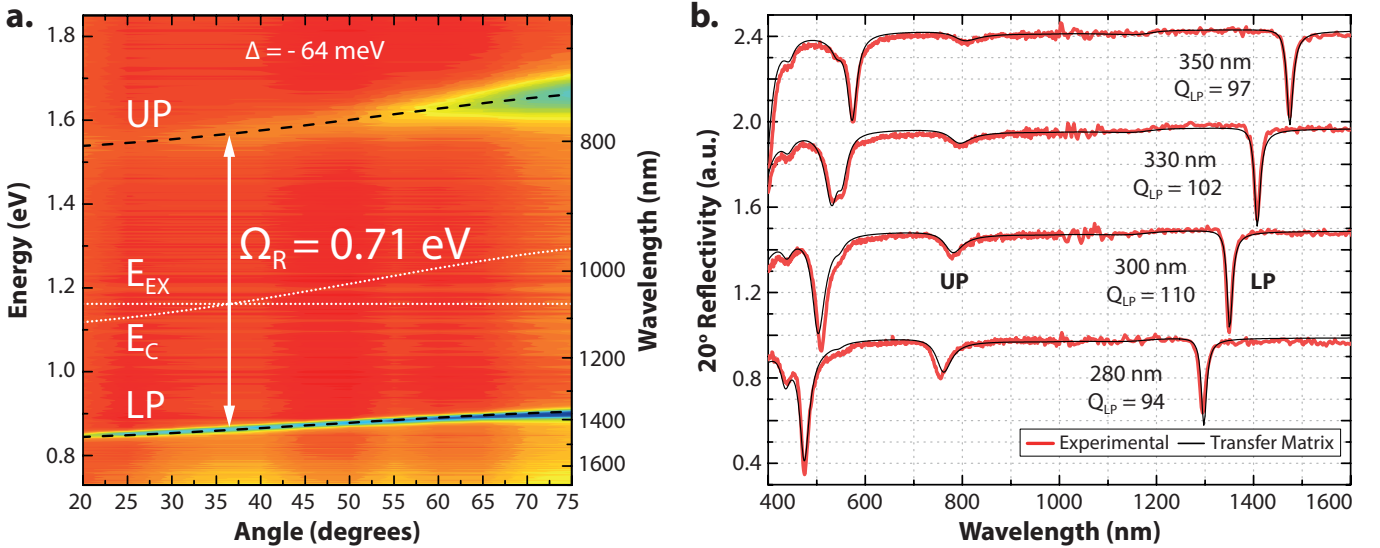


Figure 2. (a) False-color angle-dependent TM-polarized reflectivity spectrum of a 350 nm-thick microcavity. The dashed lines show the least-squares fit to the full Hopfield Hamiltonian, yielding a Rabi splitting of $\Omega_R = 0.707$ eV and a cavity energy at normal incidence of $E_C = 1.098$ eV. The detuning is $\Delta = E_C - E_{EX} = -64$ meV. (b) Measured (red) and calculated (black) TM-polarized 20° reflectivity spectra for regions of different thickness present on the same sample, as well as the experimental LP quality factors. The dip below 600 nm is the UP that originates from coupling to the second-order cavity mode.

intermolecular interactions such that the solution linear and nonlinear properties are largely preserved in high chromophore-density films.²² We show that the resulting large magnitude of the third-order susceptibility $\chi^{(3)}$ contributes to enhancing polariton-polariton interactions via the photonic component. This is used to demonstrate tunable third-harmonic generation (THG) spanning the entire visible spectrum upon resonant excitation of the LP mode. When compared to bare films, the fabricated microcavities show conversion efficiency enhancements of over two orders of magnitude and even larger internal enhancements. The structure forms a versatile platform for the study of nonlinear phenomena in the USC regime.

II. RESULTS AND DISCUSSION

To characterize the linear optical properties of the polymethine dye, neat films were prepared by spin-coating from 5-20 mg/ml dichloromethane solutions. The refractive index obtained using ellipsometry is shown in Fig. 1. The imaginary component shows a strong exciton absorption maximum at 1067 nm ($E_{EX} = 1.162$ eV) and a vibronic shoulder. Note in particular the low losses in the near-infrared part of the spectrum.

The fabricated microcavities are composed of a neat polymethine layer surrounded by silver mirrors and are shown schematically in the bottom inset of Fig. 1. To improve the wetting and optical properties of the back mirror, cleaned quartz substrates were first functionalized with a monolayer of (3-mercaptopropyl)-trimethoxysilane.²³ Then, a 75 nm-thick silver mirror was grown by thermal evaporation at a base pressure of

$\sim 10^{-7}$ mBar. After spin-coating the polymethine film, the structure was capped with a 35 nm top mirror. All of the measurements were performed at room temperature.

Figure 2 (a) shows the measured angle-resolved TM-polarized reflectivity from a 350 nm thick microcavity, which corresponds to nearly zero detuning between the exciton and photon energies at normal incidence. The dashed lines correspond to a least-squares fit to the full Hopfield Hamiltonian (see Methods),¹⁶ yielding a Rabi splitting of $\Omega_R = 0.707$ eV. A slightly larger value of $\Omega_R = 0.719$ eV is obtained for the TE-polarized reflectivity spectrum and the remaining fit parameters are summarized in Table II.

These values correspond to 60-62% of the uncoupled exciton energy, slightly exceeding the largest normalized coupling ratio (Ω_R/E_{EX}) reported to date of 60% in organic microcavities.¹⁷ The large ratio observed is a consequence of the high oscillator strength of the dye and the large number density of molecules resulting from the use of a neat film, both evidenced by the strong absorption band shown in Fig. 1. In addition, the use of metallic mirrors instead of dielectric ones leads to a reduced photonic mode volume. These two factors contribute to the increased Ω_R . Meanwhile, the near-infrared transition energy leads to a smaller E_{EX} than in previous reports. Note that for larger cavity thicknesses, the coupling ratio can exceed 90% in this structure.

We find that the experimental LP quality factors can exceed 100, which is considerably higher than typical values (below 30) obtained for all-metal microcavities.^{15,24,25} This is a consequence of the material's low linear losses and the high reflectivity of silver in the near-infrared part of the spectrum. This is helpful

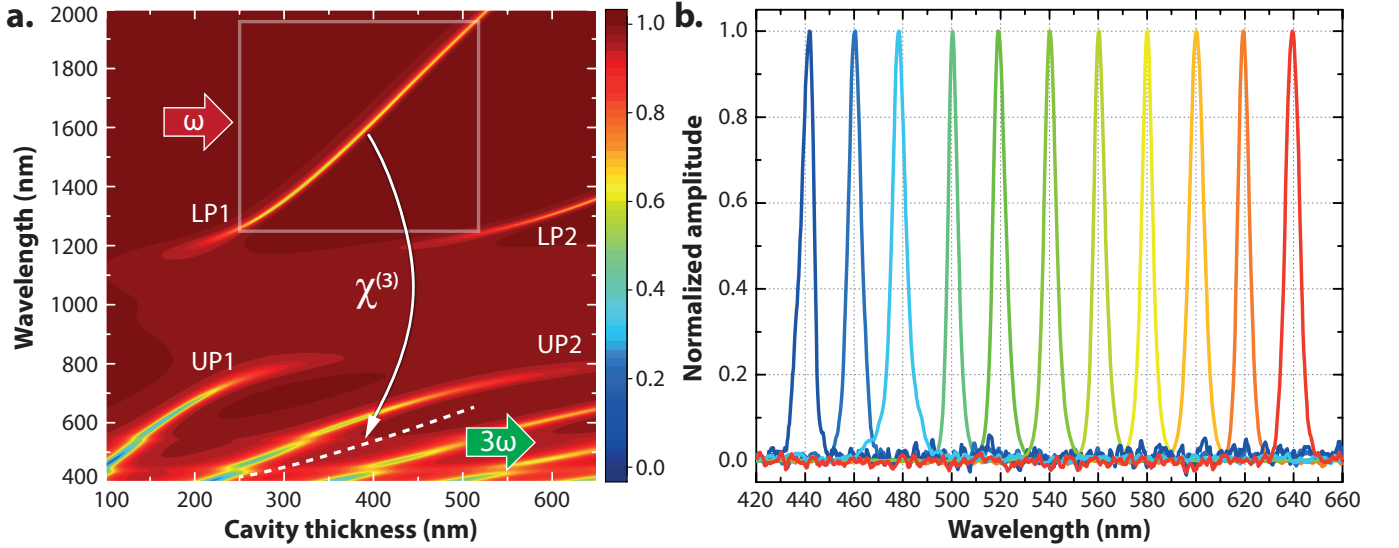


Figure 3. (a) Calculated microcavity reflectivity spectra at normal incidence for increasing values of polymethine thickness. The four polaritonic modes indicated by LP1/UP1 and LP2/UP2 arise due to the strong coupling of the exciton transition to the first- and second-order cavity modes, respectively. The top box indicates the range of LP spectral positions covered by the broad infrared pump (1250-1950 nm). The corresponding third-harmonic wavelengths are indicated by a dashed line. (b) Experimental normalized THG spectra obtained by laterally translating the same microcavity sample.

for increasing the efficiency of nonlinear processes or, in some cases, lowering their thresholds.^{26,27} Despite the inhomogeneously broadened absorption of the dye, the LP reflectivity spectra showed Lorentzian lineshapes characteristic of homogeneous broadening, a consequence of the large Rabi splitting compared to the inhomogeneous linewidth.²⁸

The LP resonance position can be readily tuned via changes in angle of incidence or sample thickness. Our use of high concentration solutions and of a high vapor pressure solvent naturally leads to large-scale thickness gradients (hundreds of microns) over the sample surface. This allows for multiple cavity thicknesses to be probed using a single sample. These can be easily identified experimentally due to changes in the surface color caused by the changing position of the UP branch. Figure 2 (b) shows a collection of measured (red) and calculated (black) TM-polarized 20° reflectivity spectra taken at different locations. The corresponding sample thicknesses are indicated below the traces.

Third-harmonic generation was first studied by exciting the sample with a broad IR pump spanning 1250-1950 nm. In the experiment, a single microscope objective is used to focus the IR pump on the sample surface and to collect the reflected third-harmonic (see Methods). Figure 3 (a) shows a calculated microcavity reflectivity map, where the spectral positions of the polariton modes are obtained for increasing values of cavity thickness. The first four polaritonic modes indicated by LP1/UP1 and LP2/UP2 correspond to strong coupling to the first- and second-order cavity modes, respectively. The broad pump is spectrally filtered by the thickness-dependent LP resonance position, as shown in the top

box in Fig. 3 (a). The resonant component is coupled into the microcavity and interacts with the high $\chi^{(3)}$ material to generate the third-harmonic signal. The THG wavelengths corresponding to the first LP branch are shown as a dashed line in the bottom of Fig. 3 (a). Figure 3 (b) shows a series of normalized THG spectra taken by laterally translating the sample and illustrates the tunability of the THG process at normal incidence. Note that the third-harmonic is not resonant with higher order modes and only light that can leak out due to the finite transmission of the mirrors is observed. Nevertheless, the generated harmonic signals were easily visible with the naked eye through the microscope optics.

To investigate the THG power dependence as a function of wavelength, the broad IR pump was spectrally filtered using 12 nm bandpass filters, which is slightly narrower than the mean LP linewidth of 14 nm obtained from Fig. 2 (b). The pump and corresponding THG wavelengths are indicated in Fig. 1 by round and triangular markers, respectively. Figure 4 shows the results obtained for the fabricated microcavities (curves 1-3). We observe a doubling of the conversion efficiency when changing from 1320 nm to 1650 nm excitation. This corresponds to an increased THG efficiency for polaritonic modes that are more photonic in nature, as highlighted in Fig. 5 (a). When pumping at 1320 nm, which corresponds to modes with a strong exciton component, we observed a fast irreversible decay of the THG signal due to sample damage — a clear signature of the mode matter content. Note, in contrast, that the linear absorption of the bare film is negligible at this wavelength. For longer wavelengths, no decrease in THG powers was observed

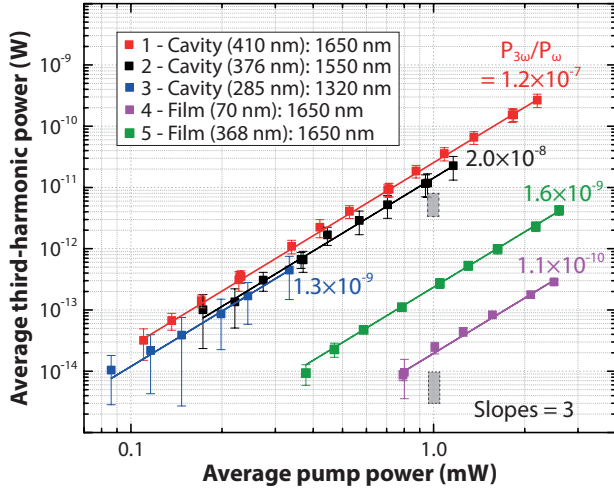


Figure 4. Measured third-harmonic powers (squares) as a function of pump power. Red, black and blue data sets correspond to microcavities pumped at 1650 nm, 1550 nm and 1320 nm, respectively. Bare polymethine films of 70 nm and 368 nm were investigated at 1650 nm and the results are shown in purple and green, respectively. The solid lines indicate a cubic power fit to each data set. The values at the end of each curve correspond to their peak conversion efficiencies, defined as $P_{3\omega}/P_{\omega}$. The top (bottom) gray boxes indicate the range of calculated reflected THG powers for the microcavity (bare films) shown in Fig. 5. The pump spot had a FWHM of 1.5 μm .

for up to an hour of measurement.

The values at the end of each curve correspond to the peak power conversion efficiencies, defined as $P_{3\omega}/P_{\omega}$. In all cases, the THG wavelength was not resonant with the higher order upper polariton modes and was not efficiently extracted from the microcavity. Nonetheless, the high experimental conversion efficiencies for the microcavities were comparable to those of other systems that required patterning or considerably thicker films.^{29–31}

For comparison, THG from bare polymethine films of different thicknesses are shown in Fig. 4 (curves 4–5). The 368 nm-thick film (curve 5) is of comparable thickness to the microcavities and allows for an accurate estimate of the conversion enhancements. Table I shows the fit coefficients C obtained by fitting each data set with a cubic power dependence of the form $P_{3\omega} = C \times P_{\omega}^3$. The last column shows the conversion enhancements with respect to the 368 nm-thick film. At the wavelength of highest conversion efficiency (1650 nm), the fabricated microcavities show raw (external) THG enhancement factors of 108 ± 1.7 compared to the bare film. As shown in Fig. 5 (a), the internal efficiency at this wavelength is approximately 50 times higher than this value due to the low fraction of THG that is out-coupled from the cavity.

Table I. Experimental cubic fit coefficients for data sets 1–5 shown in Fig. 4 and the THG conversion enhancement with respect to the 368 nm-thick bare film.

#	C	THG Enhancement
1	$(254.2 \pm 2.1) \times 10^{-4}$	108.0 ± 1.7
2	$(142.9 \pm 2.7) \times 10^{-4}$	60.7 ± 1.4
3	$(119.7 \pm 2.7) \times 10^{-4}$	50.6 ± 1.3
4	$(195.8 \pm 7.4) \times 10^{-7}$	–
5	$(235.4 \pm 3.2) \times 10^{-6}$	–

III. SIMULATIONS

To correlate our results with the LP exciton and photon fractions at normal incidence, Fig. 5 (a) shows the polariton modal content calculated using the full Hopfield Hamiltonian from experimental (circles) and simulated (squares) angle-resolved reflectivity spectra. Note that in the USC regime, the contribution from the squared electromagnetic vector potential leads to a blueshift of the bare cavity photon energy and that the modal content of both components is no longer equal at zero detuning, which corresponds to 1432 nm in Fig. 5 (a).¹² We find that the LP branch varies from 73% to 52% exciton content over the range of thicknesses used in Fig. 4 (indicated by colored arrows).

To determine the origin of the enhancement, THG was investigated using a modified transfer matrix approach, which includes nonlinear source terms.^{32–34} In this way, the combined effects of multiple reflections and absorption at both the fundamental and third-harmonic wavelengths are automatically taken into account, as well as the resonant pump enhancement and non-resonant THG extraction factors.

Figure 5 (b) shows a map of the calculated reflected THG powers for the fabricated microcavities as a function of cavity thickness and pump wavelength for an average input power of 1 mW. As expected, the THG map resembles the reflectivity map shown in the boxed region of Fig. 3 (a) because THG is only generated when the pump is resonant with the LP branch. The colored arrows indicate the experimental conditions of cavity/film thickness and pump wavelength for the measurements in Fig. 4. The top gray box in Fig. 4 shows the range of calculated reflected THG powers for the microcavities. The quantitative agreement with the experimental values is remarkable, considering that the only parameter not known with certainty is the third-order susceptibility $\chi^{(3)}(3\omega; \omega, \omega, \omega)$, which was kept dispersionless and equal to the value $\chi^{(3)}(\omega; -\omega, \omega, \omega)$ measured using the z-scan technique.²²

A similar calculation for the bare films pumped at 1650 nm is shown in the inset of Fig. 5 (b) and was found to be less accurate for the 368 nm-thick film, with the experimental value closer to the transmitted THG power (not shown) instead of the reflected one. The bottom gray box in Fig. 4 shows the range of calculated

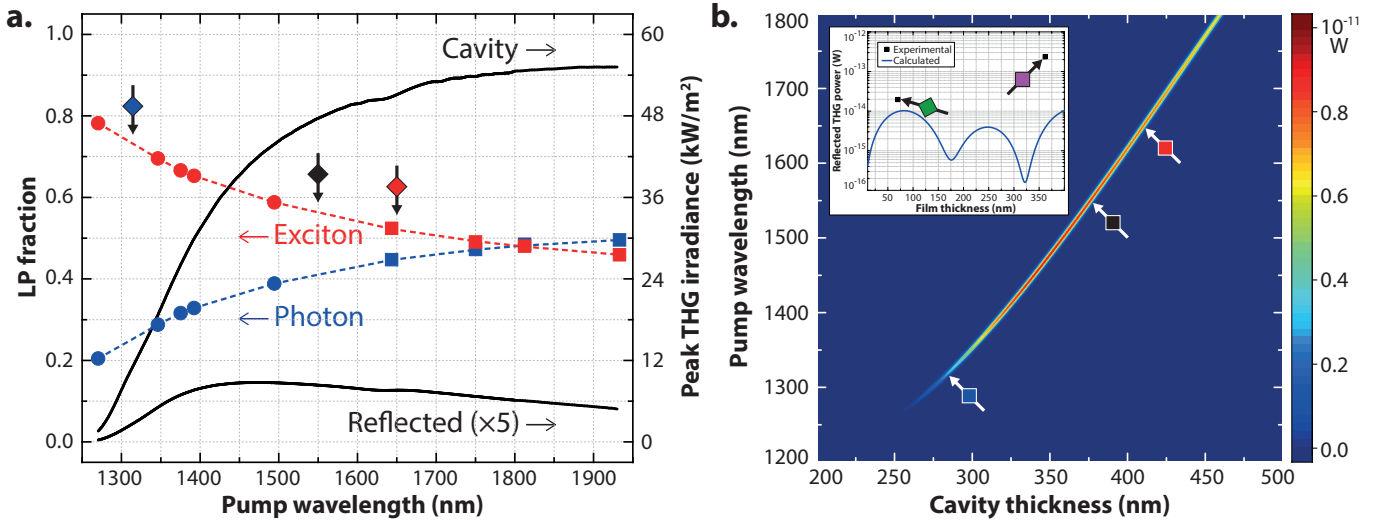


Figure 5. (a) Calculated exciton (red) and photon (blue) fractions for the first LP branch from experimental (circles) and simulated (squares) reflectivity data. The solid black curves show the calculated THG irradiances inside the cavity (top) and outside in reflection (bottom). (b) Calculated reflected third-harmonic powers as a function of microcavity thickness and pump wavelength for an average input power of 1 mW. THG is obtained when the pump is resonant with the LP mode, maintaining the same shape as in the boxed region in Fig. 3. Inset: same calculation for a thin film on quartz pumped at 1650 nm. For the calculations, $\chi^{(3)} = -5.1 \times 10^{-19}$ esu (-7.12×10^{-19} m²/V²), THG and pump spots with a FWHM of 1.5 μ m were used. The colored arrows in a,b indicate the experimental conditions for the measurements in Fig. 4.

reflected THG powers for the bare films. We believe that the discrepancy stems mostly from the large angular spread of wavevectors in the focussed pump beam, which is not accounted for in our calculations. For microcavities, wavevectors away from the resonance condition are naturally filtered out by the LP dispersion.

The agreement for the thinner film and microcavities confirm that the value of $\chi^{(3)}$ used in the calculations is a reasonable estimate for the real one. Therefore, even when neglecting possible resonant enhancements of $\chi^{(3)}$ due to the weak absorption bands in the visible part of the spectrum, the observed THG enhancements seem to be consistent with a purely (or at least mostly) photonic effect, as opposed to a drastic modification of the material's nonlinear properties.³⁵ Still, as compared to bare films, microcavities offer the advantage that they require smaller thicknesses to generate the same harmonic power. This is a consequence of the pump electric field enhancement, the reduced absorption of the generated signal and the absence of a phase-matching requirement, with the conversion efficiency depending instead on mode overlap, which can be tuned by microcavity design.³⁶

Fig. 5 (a) also shows the calculated peak THG irradiances inside the cavity as compared to the reflected THG. Both curves significantly decrease towards shorter wavelengths because of the absorption band peaked at 1067 nm. The internal THG first increases towards longer wavelengths as losses in the mirrors are reduced for thicker cavities. The decreasing transmission of the front silver mirror towards longer wavelengths eventually leads to a decrease in both the internal and reflected components, the latter already visible in Fig. 5 (a). For this

range of wavelengths, the internal THG enhancements are up to 56 times higher than the ones observed in reflection. Further calculations show that small modifications of the structure to improve out-coupling, such as reducing the top mirror thickness or achieving a doubly-resonant condition of the THG wavelength with an UP branch can further increase the THG efficiency by more than an order of magnitude.

IV. CONCLUSION

We have fabricated organic microcavities containing a nonlinear dye operating in the USC regime and possessing a normalized coupling ratio of 62%, slightly exceeding the highest value ever reported.¹⁷ The combination of the material's low losses and the use of high reflectivity silver mirrors led to LP quality factors much higher than conventional all-metal microcavities. The polariton nonlinearity was exploited to demonstrate efficient and tunable third-harmonic generation when the cavity was excited resonantly with the LP branch. Although the THG was not resonantly extracted from the microcavities, conversion enhancements of up to two orders of magnitude were obtained in comparison to bare films and transfer matrix calculations indicate that these can be understood as due to the increased pump electric field. We anticipate that this demonstration of a strong organic polariton nonlinearity will allow for the observation of novel room-temperature nonlinear effects so far restricted to low-temperature inorganic systems and new phenomena unique to the USC regime.

V. METHODS

A. Linear optical characterization

An variable-angle ellipsometer (J. A. Woollam Co., RC2 D+NIR) was used to obtain the thicknesses and optical constants of the neat polymethine films, the silver mirrors and the quartz substrate. Angle-resolved reflectivity measurements were performed using the same instrument with the help of focusing probes.

B. Fitting of the reflectivity data

The experimental Rabi splitting and mixing coefficients were extracted from the angle-resolved reflectivity data by performing a least-squares fit to the eigenvalue equation

$$\hat{H}_q \vec{v}_{j,q} = \omega_{j,q} \vec{v}_{j,q}. \quad (1)$$

\hat{H}_q is the full Hopfield Hamiltonian given by

$$\hat{H}_q = \begin{pmatrix} E_{ph}(q) + 2D & V & 2D & V \\ V & E_{EX} & V & 0 \\ -2D & -V & -E_{ph}(q) - 2D & -V \\ -V & 0 & -V & -E_{EX} \end{pmatrix}, \quad (2)$$

where $q = (\omega/c) \sin \theta$ is the in-plane wavevector, θ is the angle of incidence, $V = \Omega_R/2$ is the interaction energy and $D = V^2/E_{EX}$ is the energy contribution of the squared electromagnetic vector potential.^{12,16} The eigenvectors $\vec{v}_{j,q} = (w_{j,q}, x_{j,q}, y_{j,q}, z_{j,q})^T$ are obtained from the polariton annihilation operators

$$p_{j,q} = w_{j,q}a_q + x_{j,q}b_q + y_{j,q}a_{-q}^\dagger + z_{j,q}b_{-q}^\dagger, \quad (3)$$

where $j \in \{LP, UP\}$ and a, b are photon and exciton annihilation operators, respectively. They provide the Hopfield coefficients for the photon ($|w_{j,q}|^2$) and exciton ($|x_{j,q}|^2$) fractions as well as the anomalous coefficients ($|y_{j,q}|^2, |z_{j,q}|^2$) which only become comparable to the first ones when $\Omega_R \sim E_{EX}$.

The eigenvalues $\omega_{j,q} = \{\pm\omega_{LP,q}, \pm\omega_{UP,q}\}$ correspond to the polariton energies to be matched with the reflectivity minima. The fit parameters were the interaction energy V , the normal-incidence cavity energy E_C and the cavity's effective refractive index n_{eff} , the last two being related by

$$E_{ph}(q) = \sqrt{\left(\frac{\hbar c q}{n_{eff}}\right)^2 + E_C^2}. \quad (4)$$

The fit parameters obtained for the TE- and TM-polarized spectra are summarized in Table II.

Table II. Full Hopfield Hamiltonian fit parameters obtained for the reflectivity data of a 350 nm cavity.

Pol.	Ω_R (eV)	n_{eff}	E_C (eV)
TE	0.719 ± 0.004	1.57 ± 0.04	1.09 ± 0.01
TM	0.707 ± 0.002	1.83 ± 0.04	1.10 ± 0.01

C. Nonlinear optical characterization

Third-harmonic measurements were performed in reflection using an Olympus IX-81 inverted microscope. The samples were mounted facing an Olympus LUC-PlanFl 40 \times 0.6 NA objective with the correction collar set to zero. A supercontinuum laser (Fianium FemtoPower 1060, 40 MHz) was used as the infrared light source. The pulse duration was measured with a streak camera (Hamamatsu C10910) and found to be 48 ps. A different set of excitation (EX), beam splitter (BS) and detection (DET) filters was used for each fundamental wavelength. All filters were purchased from Thorlabs unless indicated otherwise. 1320 nm: (EX) LP1250, BP1320-12, SP1500 (Edmund Optics), 1 cm quartz cuvette with toluene; (BS) BSW29R; (DET) SP950, BP430-20 (Chroma), 1 cm quartz cuvette with water. 1550 nm: (EX) LP1250, LP1500, BP1550-12, 1 cm quartz cuvette with toluene; (BS) BSW29R; (DET) SP1500. 1650 nm: (EX) LP1250, LP1500, BP1650-12; (BS) FF538-FDi01 (Semrock); (DET) 1 cm cuvette with toluene. The transmission of all detection filters was measured and used to calibrate the measured powers.

The third-harmonic powers were measured with a cooled CCD camera (Princeton Instruments, PIXIS 400B eXcelon). The calibration procedure was performed with a 532 nm laser (supercontinuum followed by BP532-3, SP700, SP1500, 1 cm cuvette with toluene). The laser was focused on a 75-nm thick silver mirror and the reflected light was measured at the side-port of the microscope with a power meter (Thorlabs, S120VC/PM100D). Neutral-density filters with measured transmission values at 532 nm were inserted in the excitation path so that the powers at the side-port of the microscope could be adjusted in the range of $10^{-13} - 10^{-10}$ W.

For each power value, a series of images was acquired with the CCD camera and the corresponding integrated counts on two adjacent 30 \times 30 pixel regions were obtained, the first one including the laser spot and the second one only background light. The procedure was repeated for different integration times and the detector response was obtained by fitting the background-corrected counts over the known input power to a fourth-degree polynomial in integration time.

The CCD quantum efficiency is taken to remain constant in the range of THG wavelengths from 440 nm to 550 nm. The reflection collection efficiency of the objective based on the detection solid angle was estimated to be $\eta = 1 - \cos[\sin^{-1}(NA)] = 0.2$. This value only affects absolute powers, but not the enhancement factors.

ACKNOWLEDGMENTS

The authors would like to thank Johannes Feist and Simone de Liberato for helpful comments on this manuscript. FB and SKC acknowledge support from

the Natural Sciences and Engineering Research Council of Canada Discovery Grant Program, the Canada Research Chair in Hybrid and Molecular Photonics and the FQRNT PBEER scholarship program. Work at GT was supported by the Air Force Office of Scientific Research through the COMAS MURI program (agreement no. FA9550-10-1-0558).

-
- * fabio-souza.barachati@polymtl.ca
 † s.kena-cohen@polymtl.ca
- ¹ I. Carusotto and C. Ciuti, *Rev. Mod. Phys.* **85**, 299 (2013).
 - ² C. Weisbuch, M. Nishioka, A. Ishikawa, and Y. Arakawa, *Phys. Rev. Lett.* **69**, 3314 (1992).
 - ³ D. G. Lidzey, D. Bradley, M. Skolnick, T. Virgili, S. Walker, and D. Whittaker, *Nature* **395**, 53 (1998).
 - ⁴ J. J. Baumberg and P. G. Lagoudakis, *physica status solidi (b)* **242**, 2210 (2005).
 - ⁵ D. Sanvitto and S. Kéna-Cohen, *Nature Materials* **15**, 1061 (2016).
 - ⁶ J.-H. Song, Y. He, A. V. Nurmikko, J. Tischler, and V. Bulovic, *Phys. Rev. B* **69**, 235330 (2004).
 - ⁷ P. G. Savvidis, L. G. Connolly, M. S. Skolnick, D. G. Lidzey, and J. J. Baumberg, *Phys. Rev. B* **74**, 113312 (2006).
 - ⁸ S. Kéna-Cohen and S. Forrest, *Nature Photonics* **4**, 371 (2010).
 - ⁹ K. Daskalakis, S. Maier, R. Murray, and S. Kéna-Cohen, *Nature materials* **13**, 271 (2014).
 - ¹⁰ J. D. Plumhof, T. Stöferle, L. Mai, U. Scherf, and R. F. Mahrt, *Nature materials* **13**, 247 (2014).
 - ¹¹ G. Lerario, A. Fieramosca, F. Barachati, D. Ballarini, K. S. Daskalakis, L. Dominici, M. De Giorgi, S. A. Maier, G. Gigli, S. Kéna-Cohen, and D. Sanvitto, *arXiv preprint arXiv:1609.03153* (2016).
 - ¹² C. Ciuti, G. Bastard, and I. Carusotto, *Phys. Rev. B* **72**, 115303 (2005).
 - ¹³ S. De Liberato, *Phys. Rev. Lett.* **112**, 016401 (2014).
 - ¹⁴ F. Herrera and F. C. Spano, *Phys. Rev. Lett.* **116**, 238301 (2016).
 - ¹⁵ T. Schwartz, J. A. Hutchison, C. Genet, and T. W. Ebbesen, *Phys. Rev. Lett.* **106**, 196405 (2011).
 - ¹⁶ S. Kéna-Cohen, S. A. Maier, and D. D. C. Bradley, *Advanced Optical Materials* **1**, 827 (2013).
 - ¹⁷ S. Gambino, M. Mazzeo, A. Genco, O. Di Stefano, S. Savasta, S. Patanè, D. Ballarini, F. Mangione, G. Lerario, D. Sanvitto, and G. Gigli, *ACS Photonics* **1**, 1042 (2014), <http://dx.doi.org/10.1021/ph500266d>.
 - ¹⁸ J. A. Hutchison, T. Schwartz, C. Genet, E. Devaux, and T. W. Ebbesen, *Angewandte Chemie International Edition* **51**, 1592 (2012).
 - ¹⁹ J. Galego, F. J. Garcia-Vidal, and J. Feist, *Phys. Rev. X* **5**, 041022 (2015).
 - ²⁰ E. Orgiu, J. George, J. Hutchison, E. Devaux, J. Dayen, B. Doudin, F. Stellacci, C. Genet, J. Schachenmayer, C. Genes, G. Pupillo, T. Samorì, and T. Ebbesen, *Nature Materials* (2015).
 - ²¹ J. M. Hales, J. Matichak, S. Barlow, S. Ohira, K. Yesudas, J.-L. Brédas, J. W. Perry, and S. R. Marder, *Science* **327**, 1485 (2010).
 - ²² S. Barlow, J.-L. Bredas, Y. A. Getmanenko, R. L. Gieseking, J. M. Hales, H. Kim, S. R. Marder, J. W. Perry, C. Risko, and Y. Zhang, *Mater. Horiz.* **1**, 577 (2014).
 - ²³ S. Hafezian, K. Maloney, J. Lefebvre, L. Martinu, and S. Kéna-Cohen, *Applied Physics Letters* **109**, 121603 (2016), <http://dx.doi.org/10.1063/1.4963262>.
 - ²⁴ P. A. Hobson, W. L. Barnes, D. G. Lidzey, G. A. Gehring, D. M. Whittaker, M. S. Skolnick, and S. Walker, *Applied Physics Letters* **81**, 3519 (2002), <http://dx.doi.org/10.1063/1.1517714>.
 - ²⁵ S. Kéna-Cohen and S. R. Forrest, *Phys. Rev. B* **77**, 073205 (2008).
 - ²⁶ C. Ciuti, P. Schwendimann, B. Deveaud, and A. Quattropani, *Phys. Rev. B* **62**, R4825 (2000).
 - ²⁷ A. Rodriguez, M. Soljačić, J. D. Joannopoulos, and S. G. Johnson, *Opt. Express* **15**, 7303 (2007).
 - ²⁸ R. Houdré, R. P. Stanley, and M. Ilegems, *Phys. Rev. A* **53**, 2711 (1996).
 - ²⁹ M. R. Shcherbakov, D. N. Neshev, B. Hopkins, A. S. Shorokhov, I. Staude, E. V. Melik-Gaykazyan, M. Decker, A. A. Ezhov, A. E. Miroshnichenko, I. Brener, A. A. Fedyanin, and Y. S. Kivshar, *Nano Letters* **14**, 6488 (2014), pMID: 25322350, <http://dx.doi.org/10.1021/nl503029j>.
 - ³⁰ G. Ramos-Ortiz, M. Cha, S. Thayumanavan, J. C. Mendez, S. R. Marder, and B. Kippelen, *Applied Physics Letters* **85**, 179 (2004), <http://dx.doi.org/10.1063/1.1771809>.
 - ³¹ G. Grinblat, Y. Li, M. P. Nielsen, R. F. Oulton, and S. A. Maier, *Nano Letters* **16**, 4635 (2016), pMID: 27331867, <http://dx.doi.org/10.1021/acs.nanolett.6b01958>.
 - ³² D. S. Bethune, *J. Opt. Soc. Am. B* **6**, 910 (1989).
 - ³³ A. Rose, S. Larouche, D. Huang, E. Poutrina, and D. R. Smith, *Phys. Rev. E* **82**, 036608 (2010).
 - ³⁴ F. Barachati, S. De Liberato, and S. Kéna-Cohen, *Phys. Rev. A* **92**, 033828 (2015).
 - ³⁵ T. Chervy, J. Xu, Y. Duan, C. Wang, L. Mager, M. Frerejean, J. A. W. Munninghoff, P. Tinnemans, J. A. Hutchison, C. Genet, A. E. Rowan, T. Rasing, and T. W. Ebbesen, *Nano Letters* **16**, 7352 (2016), pMID: 27960510, <http://dx.doi.org/10.1021/acs.nanolett.6b02567>.
 - ³⁶ I. B. Burgess, Y. Zhang, M. W. McCutcheon, A. W. Rodriguez, J. Bravo-Abad, S. G. Johnson, and M. Lončar, *Opt. Express* **17**, 20099 (2009).